

The role of nuclear reactions and α -particle transport in the dynamics of inertial confinement fusion capsules

Josselin Garnier^{1,a)} and Catherine Cherfils-Cl  rouin²

¹Laboratoire de Probabilit  s et Mod  les Al  atoires and Laboratoire Jacques-Louis Lions, Universit   Paris VII, 2 Place Jussieu, 75251 Paris Cedex 05, France

²Commissariat    l'  nergie Atomique, Direction des Applications Militaires, Bo  te Postale 12, 91680 Bruy  res le Ch  tel, France

(Received 21 April 2008; accepted 27 August 2008; published online 7 October 2008)

This paper is devoted to the study of the deceleration phase of inertial confinement capsules. The purpose is to obtain a zero-dimensional model that has the form of a closed system of ordinary differential equations for the main hydrodynamic quantities. The model takes into account the energy released by nuclear reactions, a nonlocal model for the α -particle energy deposition process, and radiation loss by electron bremsstrahlung. The asymptotic analysis is performed in the case of a strong temperature dependence of the thermal conductivity. We finally study the beginning of the expansion phase after stagnation to derive an ignition criterion.    2008 American Institute of Physics. [DOI: 10.1063/1.2988333]

I. INTRODUCTION

In this paper, we address the deceleration phase of an inertial confinement fusion (ICF) capsule. In ICF, a spherical capsule of cryogenic deuterium-tritium (DT) fuel and filled with gaseous DT is imploded by laser or x-ray irradiation.¹ A series of shocks driven by the irradiation and reflected off the center and the shell inner surface increase the pressure of the low-density gaseous hot spot enclosed by the shell. When the pressure is large enough, the deceleration phase develops at the shell inner surface. In Refs. 2 and 3, Betti *et al.* proposed a self-similar analysis of the hot spot dynamics in the quasi-isobaric approach. This work has been extended to take into account a refined shell model, and the linear stability of the self-similar solution has been analyzed in Refs. 4–6. These results are important because the numerical simulations of the final steps of an ICF capsule implosion are very costly. A zero-dimensional model is therefore an important tool for target design and optimization. Besides, the linear stability analysis of this explicit spherical flow is an analytic tool for the study of Rayleigh–Taylor instability.

However, the description of the nuclear reactions is very crude in these models. Indeed, in Refs. 2–6, the nuclear reaction rate is assumed to be uniform in the hot spot and the energy deposition process by the generated α -particles is assumed to be local. This has been found to significantly impact the burn process of ICF targets.⁷ Here we pay particular attention to the modeling of the nuclear reaction rate on the one hand and of the energy deposition by the α -particles on the other hand. It is possible to deal with a general form of the fusion cross section and a quite general α -particle transport model in the asymptotic framework where the heat conductivity has a strong temperature dependence. More exactly, we consider a Spitzer law for heat conductivity of the form χT^ν , and we perform a careful asymptotic analysis in the

limit $\nu \gg 1$. The predictions of the asymptotic analysis are checked and validated in the case $\nu=5/2$ considered in Refs. 2–5. The idea to perform an asymptotic analysis $\nu \gg 1$ was used before to study Rayleigh–Taylor unstable ablation fronts encountered in ICF in Ref. 8 and can be found also in Ref. 9. A similar strategy was applied to the study of diffusive x-ray-driven heat waves in Ref. 10. Here we show that it allows us to recover the results obtained in previous works using self-similar solutions, and that it can be extended to more general cases in which self-similar solutions do not exist.

The paper is organized as follows. We describe the model in Sec. II A. The asymptotic analysis is performed in Sec. III. In Sec. IV, we derive the effective zero-dimensional system that we discuss in detail. In Sec. V, we study the expansion phase in order to derive an ignition criterion in terms of accessible quantities.

II. THE MODEL

A. Conservation equations

The model is based on the mass, momentum, and energy conservation equations

$$\partial_t(\rho) + \nabla \cdot (\rho \mathbf{u}) = 0, \quad (1)$$

$$\partial_t(\rho \mathbf{u}) + \nabla \cdot (\rho \mathbf{u} \otimes \mathbf{u}) + \nabla p = 0, \quad (2)$$

$$\begin{aligned} \partial_t(\rho) + \gamma p \nabla \cdot \mathbf{u} + \mathbf{u} \cdot \nabla p - (\gamma - 1) \nabla \cdot [\kappa(T) \nabla T] \\ = (\gamma - 1)(S - B), \end{aligned} \quad (3)$$

where S is the source term given by the energy deposited by the α -particles generated by nuclear reactions. $B = a_b \rho^2 T^{1/2}$ is the radiative loss due to electron bremsstrahlung. $\kappa(T) = \chi T^\nu$ is the Spitzer thermal conductivity. This system is completed by the standard ideal gas equation of state (EOS) $p = (\gamma - 1) C_v \rho T$, with $\gamma = 5/3$ for a monatomic gas. C_v is the specific heat at constant volume.

^{a)}URL: <http://www.proba.jussieu.fr/~garnier>. Electronic mail: garnier@math.jussieu.fr.

For subsonic flows, the solution of the equations of motion can be expanded in powers of the Mach number. To lowest order, we get the flat pressure approximation $p(t, \mathbf{r}) = p_h(t)$. To order one, the mass and energy conservation equations read in spherical geometry as

$$\frac{\partial \rho}{\partial t} + \frac{1}{r^2} \frac{\partial}{\partial r} (r^2 \rho u) = 0, \quad (4)$$

$$\begin{aligned} \dot{p}_h + \frac{\gamma p_h}{r^2} \frac{\partial}{\partial r} (r^2 u) - \frac{\chi(\gamma-1)}{r^2} \frac{\partial}{\partial r} \left[r^2 T^{\nu} \frac{\partial}{\partial r} (T) \right] \\ = (\gamma-1)(S-B), \end{aligned} \quad (5)$$

where the dot stands for a time derivative. The momentum equation describes the spatial fluctuations of the pressure and it can be integrated *a posteriori*. The right-hand side of the energy conservation equation (5) is described in the next subsection.

B. Source term

The source term S in the energy conservation equation can be determined by analyzing the nuclear reaction rate on the one hand and the α -particles energy deposition process on the other hand. The nuclear reaction rate is $S_{\alpha}(r, t) = \rho^2 E_{\alpha} \langle \sigma v \rangle / (4m_i^2)$, where E_{α} is the α -particle energy, $\langle \sigma v \rangle$ is the fusion reaction rate, and m_i is the ion mass. We write the fusion cross section as $\langle \sigma v \rangle = S_{\alpha} T^2 f_{\alpha}(T)$, where f_{α} is a given function of the temperature (see Appendix A). As a result, the nuclear reaction rate is spatial and time-dependent,

$$S_{\alpha}(r, t) = \mu_{\alpha} \rho_h^2(t) f_{\alpha}[T(r, t)], \quad \mu_{\alpha} = \frac{S_{\alpha} A_{\alpha}}{(\gamma-1)^2 C_v^2},$$

with $A_{\alpha} = E_{\alpha} / (4m_i^2)$. Here we have used the ideal gas EOS and the isobaric approximation $p_h = (\gamma-1) C_v \rho T$. Note that if we can approximate the fusion cross section by a quadratic form $\langle \sigma v \rangle \approx S_{\alpha} T^2$, i.e., $f_{\alpha} = 1$, then the nuclear reaction rate is spatially uniform. Such an approximation is valid if $6 < T < 20$ keV (Ref. 2) and it was also used in Refs. 4 and 5. However, at low temperatures the model is not correct. Therefore, the border of the hot spot, where the temperature becomes small, is poorly characterized. We shall consider the general model with an arbitrary function $f_{\alpha}(T)$ in this paper.

The source term $S(r, t)$ is not equal to $S_{\alpha}(r, t)$ in general, because the α -particles generated by the nuclear reactions do not deliver their energy locally. We can write

$$S(r, t) = \mathcal{P}_{\alpha}(t) \Theta(r, t),$$

where $\mathcal{P}_{\alpha}(t)$ is the total power produced by the nuclear reactions inside the hot spot,

$$\mathcal{P}_{\alpha}(t) = 4\pi \int_0^{R_h(t)} S_{\alpha}(r, t) r^2 dr.$$

In the case of local energy deposition, we have $S = S_{\alpha}$ and $\Theta(r, t) = S_{\alpha}(r, t) / \mathcal{P}_{\alpha}(t)$. In general, the computation of Θ requires an energy deposition model. In this paper, we use the model described in Ref. 1, Sec. 4.1.2, which is valid for a DT plasma at temperatures below 25–30 keV. In this regime,

the largest contribution to α -particle stopping comes from small-angle collisions with electrons. The α -particles are generated inside the hot spot, with the generation rate $S_{\alpha}(r, t) / E_{\alpha}$. Their initial velocity is $v_{\alpha 0}$ such that $E_{\alpha} = m_i v_{\alpha 0}^2 / 2$ and their initial direction is uniform on the unit sphere. The α -particles move along (nearly) straight paths and their velocity decreases according to

$$\frac{dv_{\alpha}}{dt} = -\frac{v_{\alpha}}{2t_{\alpha e}}, \quad (6)$$

where $t_{\alpha e} = (c_{\alpha e} T^{\nu-1}) / (\rho \ln \Lambda_{\alpha e})$ is a characteristic time for energy deposition and $\ln \Lambda_{\alpha e}$ is the Coulomb logarithm for collisions between α -particles and electrons. In this paper, we assume that $\ln \Lambda_{\alpha e}$ is constant, so that

$$t_{\alpha e} = \frac{c_{\alpha e} C_v (\gamma-1) T^{\nu}}{\ln \Lambda_{\alpha e} p_h},$$

where we have used the ideal-gas equation of state. Here we deal with a nonstationary, nonuniform plasma, so that the integration of Eq. (6), which in turn gives the function Θ , is not straightforward. However, it is possible to simplify the problem significantly. Indeed, the energy deposition process has two successive steps: First, the α -particles deliver energy to electrons with the characteristic time $t_{\alpha e}$; second, the electrons equilibrate with the ions with the characteristic time t_{ei} . The latter process is local. In this paper, we assume that $t_{\alpha e}$ and t_{ei} are much smaller than the characteristic time scale of evolution of the hydrodynamic quantities. Therefore, for any time t_0 , we need to solve Eq. (6) with the frozen temperature profile $T(t_0, r)$ and pressure $p_h(t_0)$.

The power radiated by electron bremsstrahlung is modeled by the term $B = a_b \rho^2 T^{1/2}$. This formula is correct as long as the plasma is optically thin, which holds true when R_h is smaller than the Planck mean free path l_p . For equimolar DT, we have $l_p = \lambda_p T^{7/2} \rho^{-2}$ (Ref. 1, Sec. 4.1.5) and the condition $R_h \ll l_p$ is always satisfied by the hot spot. In the quasi-isobaric approximation, we have $\rho = p_h / [C_v (\gamma-1) T]$ so that the power radiated by bremsstrahlung takes the form

$$B(r, t) = \mu_{\beta} \rho_h^2(t) T^{-3/2}(r, t), \quad \mu_{\beta} = \frac{a_b}{C_v^2 (\gamma-1)^2}.$$

The total power radiated by electron bremsstrahlung is

$$\mathcal{P}_{\beta}(t) = 4\pi \int_0^{R_h(t)} B(r, t) r^2 dr.$$

C. The invariant

As shown in Refs. 2 and 4, the temperature becomes evanescent at the edge $r = R_h(t)$ of the hot spot, which shows that the α -particles are stopped within the hot spot. Consequently, the power produced by the nuclear reactions inside the hot spot is totally deposited inside the hot spot, so that the total nuclear power deposited inside the hot spot is

$$4\pi \int_0^{R_h(t)} S(r, t) r^2 dr = \mathcal{P}_{\alpha}(t),$$

and therefore the function Θ must satisfy

$$4\pi \int_0^{R_h(t)} \Theta(r,t) r^2 dr = 1. \quad (7)$$

As shown in Refs. 2 and 4 and in Sec. III D, (i) the temperature and the heat flux are evanescent at the edge of the hot spot; (ii) the fluid velocity at R_h is the sum of the surface motion and the ablative flow $u(R_h(t), t) = \dot{R}_h(t) + V_{\text{loc}}(t)$, and the local ablation velocity $V_{\text{loc}}(t)$ is much smaller than the interface velocity. By multiplying Eq. (5) by $4\pi r^2$ and by integrating from 0 to R_h , we obtain

$$4\pi \left[\frac{R_h^3}{3} \dot{p}_h + \gamma p_h R_h^2 \dot{R}_h \right] = (\gamma - 1) [\mathcal{P}_\alpha - \mathcal{P}_\beta]. \quad (8)$$

In the absence of nuclear reaction and bremsstrahlung, this identity shows the existence of the invariant $p_h(t) R_h^{3\gamma}(t)$.^{2,11}

D. Temperature profile

The energy conservation equation can be integrated to obtain an expression of the velocity flow. Substituting into the mass conservation equation and eliminating the density by using the EOS, we get the equation governing the evolution of the temperature. If we introduce

$$T(r,t) = T_c(t) \phi^{1/\nu} \left[\frac{r}{R_h(t)}, t \right], \quad (9)$$

$$\Theta(r,t) = \frac{1}{R_h^3(t)} \theta \left[\frac{r}{R_h(t)}, t \right],$$

with $\phi(0,t)=1$ and $T_c(t)$ the central hot spot temperature, then the equation for the temperature reads

$$\begin{aligned} & \left[\dot{p}_h T_c + \left(\frac{\mathcal{P}_\alpha}{R_h^3} \theta - \frac{\mathcal{P}_\beta}{R_h^3} \theta_b \right) T_c - \frac{\gamma p_h}{\gamma - 1} \dot{T}_c \right] \phi^{1/\nu} \\ & - \left[\frac{\gamma p_h}{\gamma - 1} T_c \right] \frac{\partial \phi^{1/\nu}}{\partial t} + \left[\frac{\chi T_c^{\nu+2}}{\nu R_h^2} \right] \frac{\phi^{2/\nu}}{\eta^2} \frac{\partial}{\partial \eta} \left(\eta^2 \frac{\partial \phi}{\partial \eta} \right) \\ & + \left[\frac{\mathcal{P}_\alpha}{R_h^3} T_c \left(\frac{\eta}{4\pi} - \frac{1}{\eta^2} \bar{\theta} \right) - \frac{\mathcal{P}_\beta}{R_h^3} T_c \left(\frac{\eta}{4\pi} - \frac{1}{\eta^2} \bar{\theta}_b \right) \right] \frac{\partial \phi^{1/\nu}}{\partial \eta} = 0, \end{aligned} \quad (10)$$

where

$$\theta_b(\eta, t) = b_\nu^{-1}(t) \phi^{-3/(2\nu)}(\eta, t),$$

$$b_\nu(t) = 4\pi \int_0^1 \phi^{-3/(2\nu)}(\eta, t) \eta^2 d\eta,$$

$$\bar{\theta}(\eta, t) = \int_0^\eta s^2 \theta(s, t) ds, \quad \bar{\theta}_b(\eta, t) = \int_0^\eta s^2 \theta_b(s, t) ds.$$

Note that $4\pi \bar{\theta}(1, t) = 1$ and $4\pi \bar{\theta}_b(1, t) = 1$. In the absence of bremsstrahlung and nuclear reactions (or in the presence of nuclear reactions with a quadratic fusion reaction rate and a local deposition process), it is possible to find a family of self-similar solutions to Eq. (10).^{2,4} Unfortunately, the general model considered in this paper leads to an equation that does not support self-similar solutions. In the next section,

we will carry out an analysis based on asymptotic expansions with respect to the parameter ν , which is supposed to be large. The self-similar solutions exhibited in Refs. 2 and 4 will then serve as reference solutions to check that the asymptotic expansion of the solution derived in this paper is in agreement with the self-similar solutions in the special cases in which these solutions are supported. This will give an indication of the values for the parameter ν for which the asymptotic theory is valid.

III. HOT SPOT DYNAMICS

A. The large- ν limit

In the limit $\nu \gg 1$, we can neglect the variations of $\phi^{1/\nu}$ compared to the variations of ϕ at lowest order. As a consequence, we can simplify Eq. (10) by setting $\phi^{1/\nu} \simeq 1$ and we get the simplified equation

$$\begin{aligned} & \left[\dot{p}_h T_c - \frac{\gamma p_h}{\gamma - 1} \dot{T}_c \right] + \left[\frac{\chi T_c^{\nu+2}}{\nu R_h^2} \right] \frac{1}{\eta^2} \frac{\partial}{\partial \eta} \left(\eta^2 \frac{\partial \phi}{\partial \eta} \right) \\ & = \frac{3}{4\pi} \frac{\mathcal{P}_\beta}{R_h^3} T_c - \frac{\mathcal{P}_\alpha}{R_h^3} T_c \theta. \end{aligned} \quad (11)$$

We deal with the source term perturbatively as well: in a first step, we simplify it by assuming that θ is uniform, that is, by setting $\theta = 3/(4\pi)$. This is fair as the temperature is low at the beginning of the deceleration phase, so that α -particles deposit their energy locally. This gives

$$\begin{aligned} & \left[\dot{p}_h T_c + \frac{3}{4\pi} \left(\frac{\mathcal{P}_\alpha}{R_h^3} - \frac{\mathcal{P}_\beta}{R_h^3} \right) T_c - \frac{\gamma p_h}{\gamma - 1} \dot{T}_c \right] \\ & + \left[\frac{\chi T_c^{\nu+2}}{\nu R_h^2} \right] \frac{1}{\eta^2} \frac{\partial}{\partial \eta} \left(\eta^2 \frac{\partial \phi}{\partial \eta} \right) = 0. \end{aligned} \quad (12)$$

The resolution of this equation leads to a first approximation of the temperature profile T , which in turn will allow us to compute an approximated nuclear power deposition profile θ . In a second step, we will substitute the approximated nuclear power deposition and temperature profiles in Eq. (10) to get a more accurate solution.

The integration of Eq. (12) using the boundary conditions $\phi(0, t) = 1$ and $\phi(1, t) = 0$ gives the zero-order approximation

$$\phi_0(\eta) = 1 - \eta^2. \quad (13)$$

B. The nuclear power deposition profile

In this subsection, we compute the function $\theta(\eta, t)$ that is the power density profile deposited by the α -particles in the inhomogeneous plasma whose temperature profile corresponds to Eq. (13),

$$T^\nu(t, r) = T_c^\nu(t) \left[1 - \frac{r^2}{R_h^2(t)} \right]. \quad (14)$$

In a first step, we will study the evolution of an α -particle

and show how it deposits its energy in the hot spot. In a second step, we will compute the nuclear power deposition profile, which is an integration of the first step with respect to the α -particle generation rate.

The first step is carried out in Appendix B. It is remarkable that analytical calculations can be carried out, which is a consequence of the particular form (14) of the inhomogeneous plasma. For the second step, we note that the nuclear reaction rate in the inhomogeneous plasma with the temperature profile (14) is

$$S_\alpha(r, t) = \frac{1}{R_h^3(t)} \theta_\alpha \left(\frac{r}{R_h(t)}, t \right) \mathcal{P}_\alpha(t), \quad (15)$$

$$\theta_\alpha(\eta, t) = \frac{f_\alpha[T_c(t)(1 - \eta^2)^{1/\nu}]}{4\pi \int_0^1 f_\alpha[T_c(t)(1 - \eta_0^2)^{1/\nu}] \eta_0^2 d\eta_0}, \quad (16)$$

where the total nuclear power is

$$\mathcal{P}_\alpha(t) = 4\pi \mu_\alpha R_h^3(t) p_h^2(t) \int_0^1 f_\alpha[T_c(t)(1 - \eta^2)^{1/\nu}] \eta^2 d\eta. \quad (17)$$

The α -particles are emitted in the hot spot, that is, the ball with center 0 and radius R_h , with the production rate $S_\alpha(r, t)/E_\alpha$ and with a direction uniformly chosen on the unit sphere. By integrating the energy deposited by an α -particle over the distribution of particles generated by nuclear reactions, we obtain that the power deposited in the annulus $[r, r+dr]$ is $4\pi r^2 S(r, t) dr$, where the power density is

$$S(r, t) = \frac{1}{R_h^3(t)} \theta \left(\frac{r}{R_h(t)}, t \right) \mathcal{P}_\alpha(t), \quad (18)$$

$$\theta(\eta, t) = \frac{1}{2\eta^2} \int_0^\pi \int_0^{2\pi} \tilde{e}(\eta; \eta_0, t, \psi) \theta_\alpha(\eta_0, t) \eta_0^2 \sin \psi d\eta_0 d\psi, \quad (19)$$

and \tilde{e} is computed in Appendix B. The time dependence of $\theta(\eta, t)$ is through $M(t)$ and $T_c(t)$ only. The important parameter $M(t)$ is defined by

$$M(t) = \frac{2v_{\alpha 0} t_{ae}(t)}{R_h(t)} = \frac{2v_{\alpha 0} c_{ae} C_v (\gamma - 1)}{\ln \Lambda_{ae}} \frac{T_c^\nu(t)}{R_h(t) p_h(t)}, \quad (20)$$

where $v_{\alpha 0}$ is the initial velocity of the α -particles. The parameter $M(t)$ is a quantity that depends only on $R_h(t)$, $p_h(t)$, and $T_c(t)$. It is proportional to the ratio of the expected mean free path of an α -particle over the radius of the hot spot.

From the practical point of view, the evaluation of the double integral (19) is performed after the change of variables $x = \eta_0 \cos \psi$, $y = \eta_0 \sin \psi$, which gives

$$\theta(\eta, t) = \theta_0[\eta, M(t), T_c(t)], \quad (21)$$

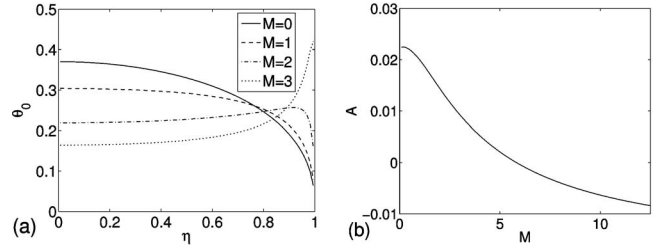


FIG. 1. (a) Nuclear power deposition profiles $\theta_0(\eta, M, T)$ for different values of M , $\nu=5/2$, and $f_\alpha(T)=f_1 T$. (b) Function $M \mapsto A_\nu(M, T)$ for $\nu=5/2$ and $f_\alpha(T)=f_1 T$.

$$\theta_0(\eta, M, T) = \frac{1}{4\pi \eta^2} \frac{\int_D \check{e}(\eta; x, y, M) f_\alpha[T(1 - x^2 - y^2)^{1/\nu}] y dx dy}{\int_D f_\alpha[T(1 - x^2 - y^2)^{1/\nu}] y dx dy}, \quad (22)$$

where D is the half-disk $\{(x, y) \in \mathbb{R}^2, y \geq 0, x^2 + y^2 \leq 1\}$ and

$$\begin{aligned} \check{e}(\eta; x, y, M) = & \frac{2}{M} \frac{\eta}{(1 - \eta^2) \sqrt{\eta^2 - y^2}} \\ & \times \{ \mathbf{1}_{x \geq 0} \check{v}_+(\eta) \mathbf{1}_{[\sqrt{x^2+y^2}, \eta_{\text{pl}}]}(\eta) \\ & + \mathbf{1}_{x \leq -\sqrt{1-y^2} \tanh(M\sqrt{1-y^2})} \check{v}_-(\eta) \mathbf{1}_{[\eta_{\text{pl}}, \sqrt{x^2+y^2}]}(\eta) \\ & + \mathbf{1}_{-\sqrt{1-y^2} \tanh(M\sqrt{1-y^2}) < x < 0} [\check{v}_+(\eta) \mathbf{1}_{[y, \eta_{\text{pl}}]}(\eta) \\ & + \check{v}_-(\eta) \mathbf{1}_{[y, \sqrt{x^2+y^2}]}(\eta)] \}, \end{aligned}$$

$$\begin{aligned} \check{v}_+(\eta; x, y, M) = & 1 - \frac{1}{M\sqrt{1-y^2}} \\ & \times \operatorname{arctanh} \left[\frac{\sqrt{1-y^2}(x - \sqrt{\eta^2 - y^2})}{x\sqrt{\eta^2 - y^2} - (1 - y^2)} \right], \end{aligned}$$

$$\begin{aligned} \check{v}_-(\eta; x, y, M) = & 1 + \frac{1}{M\sqrt{1-y^2}} \\ & \times \operatorname{arctanh} \left[\frac{\sqrt{1-y^2}(x + \sqrt{\eta^2 - y^2})}{x\sqrt{\eta^2 - y^2} + (1 - y^2)} \right], \end{aligned}$$

$$\eta_f^2(x, y, M) = y^2 + (1 - y^2) \left\{ \frac{x + \sqrt{1-y^2} \tanh[\sqrt{1-y^2} M]}{x \tanh[\sqrt{1-y^2} M] + \sqrt{1-y^2}} \right\}^2.$$

If $M \ll 1$, then the energy deposition can be considered as local and the power density profile satisfies $\theta \approx \theta_\alpha$, which reads

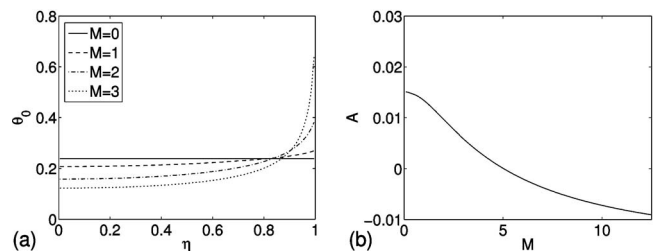


FIG. 2. The same as in Fig. 1, but $f_\alpha(T)=f_0$.

$$\theta_0(\eta, M, T) \simeq \frac{M^{\leq 1}}{4\pi} \frac{1}{\int_0^1 f_\alpha [T(1-\eta^2)^{1/\nu}] \eta_0^2 d\eta_0} f_\alpha [T(1-\eta^2)^{1/\nu}]$$

If $M \gg 1$, then the energy is deposited in a thin layer at the edge of the hot spot, so that the power deposition profile θ_0 is concentrated around $\eta=1$ [see Figs. 1(a) and 2(a)].

Whatever the values of M and T are, we have by Eq. (7) $4\pi \int_0^1 \theta_0(\eta, M, T) \eta^2 d\eta = 1$.

C. The temperature profile

We substitute the zero-order expressions (21) for θ and $(1-\eta^2)^{1/\nu}$ for $\phi^{1/\nu}$ into Eq. (10), which gives the equation

$$\begin{aligned} & \left[\dot{p}_h T_c - \frac{\gamma P_h}{\gamma-1} \dot{T}_c \right] (1-\eta^2)^{1/\nu} - \frac{2\mathcal{P}_\alpha T_c}{\nu R_h^3} \left(\frac{\eta}{4\pi} - \frac{1}{\eta^2} \int_0^\eta \theta_0(s, M, T_c) s^2 ds \right) \eta (1-\eta^2)^{-1+1/\nu} \\ & + \frac{2\mathcal{P}_\beta T_c}{\nu R_h^3} \left(\frac{\eta}{4\pi} - \frac{1}{b_\nu \eta^2} \int_0^\eta (1-s^2)^{-3/(2\nu)} s^2 ds \right) \eta (1-\eta^2)^{-1+1/\nu} + \left[\frac{\chi T_c^{\nu+2}}{\nu R_h^2} \right] \frac{(1-\eta^2)^{2/\nu}}{\eta^2} \frac{\partial}{\partial \eta} \left(\eta^2 \frac{\partial \phi}{\partial \eta} \right) \\ & = - \frac{\mathcal{P}_\alpha}{R_h^3} T_c \theta_0(\eta, M, T_c) (1-\eta^2)^{1/\nu} + \frac{\mathcal{P}_\beta}{R_h^3} T_c b_\nu^{-1} (1-\eta^2)^{-1/(2\nu)}, \end{aligned} \tag{23}$$

with

$$b_\nu = 4\pi \int_0^1 (1-\eta^2)^{-3/(2\nu)} \eta^2 d\eta = \pi^{3/2} \frac{\Gamma\left(1 - \frac{3}{2\nu}\right)}{\Gamma\left(\frac{5}{2} - \frac{3}{2\nu}\right)}, \tag{24}$$

$$\mathcal{P}_\beta(t) = \mu_\beta b_\nu p_h^2(t) R_h^3(t) T_c^{-3/2}(t).$$

Multiplying by $\eta^2(1-\eta^2)^{-2/\nu}$, integrating twice with respect to η , and using the boundary conditions $\phi(0, t)=1$ and $\phi(1, t)=0$, we obtain the time evolution equation of the central temperature

$$\begin{aligned} & \left[\dot{p}_h T_c - \frac{\gamma P_h}{\gamma-1} \dot{T}_c \right] c_\nu - \frac{\chi T_c^{\nu+2}}{\nu R_h^2} \\ & = - \frac{\mathcal{P}_\alpha}{R_h^3} T_c A_\nu(M, T_c) + \frac{\mathcal{P}_\beta}{R_h^3} T_c d_\nu, \end{aligned} \tag{25}$$

with

$$c_\nu = \frac{\nu}{2(\nu-1)} - \frac{\sqrt{\pi} \Gamma\left(1 - \frac{1}{\nu}\right)}{4\Gamma\left(\frac{5}{2} - \frac{1}{\nu}\right)}, \tag{26}$$

$$\begin{aligned} A_\nu(M, T) &= \int_0^1 s^2 \theta_0(s, M, T) \int_s^1 \frac{(1-u^2)^{-1/\nu}}{u^2} dud s \\ &= \frac{1}{2\pi} \left[\frac{3\sqrt{\pi} \Gamma\left(1 - \frac{1}{\nu}\right)}{8\Gamma\left(\frac{5}{2} - \frac{1}{\nu}\right)} - \frac{\nu}{2(\nu-1)} \right], \end{aligned} \tag{27}$$

$$\begin{aligned} d_\nu &= \frac{1}{b_\nu} \int_0^1 s^2 (1-s^2)^{-3/(2\nu)} \int_s^1 \frac{(1-u^2)^{-1/\nu}}{u^2} dud s \\ &= \frac{1}{2\pi} \left[\frac{3\sqrt{\pi} \Gamma\left(1 - \frac{1}{\nu}\right)}{8\Gamma\left(\frac{5}{2} - \frac{1}{\nu}\right)} - \frac{\nu}{2(\nu-1)} \right]. \end{aligned} \tag{28}$$

In the case in which $f_\alpha(T)$ is a power law, $f_\alpha(T) \sim T^n$, then θ_0 and A_ν do not depend on T . The function $A_{5/2}$ is plotted in Fig. 1(b) ($n=1$) and Fig. 2(b) ($n=0$). In particular, $A_{5/2} \rightarrow -0.0179$ as $M \rightarrow \infty$. We also have $b_{5/2}=12.84$, $c_{5/2}=0.203$, and $d_{5/2}=0.0162$.

Finally, substituting Eq. (25) into Eq. (23), we obtain the temperature profile at first order,

$$\begin{aligned} \phi_1(\eta, t) &= 1 + \frac{1}{c_\nu} \left(\frac{\nu \mathcal{P}_\alpha A_\nu(M, T_c)}{\chi T_c^{\nu+1} R_h} - \frac{\nu \mathcal{P}_\beta d_\nu}{\chi T_c^{\nu+1} R_h} - 1 \right) \int_0^\eta s \left(1 - \frac{s}{\eta} \right) (1-s^2)^{-1/\nu} ds \\ &+ \frac{\nu \mathcal{P}_\alpha}{\chi T_c^{\nu+1} R_h} \left\{ \frac{1}{2\pi \nu} \int_0^\eta s^3 \left(1 - \frac{s}{\eta} \right) (1-s^2)^{-1-1/\nu} ds - \int_0^\eta s^2 \theta_0(s, M, T_c) \int_s^\eta \frac{(1-u^2)^{-1/\nu}}{u^2} dud s \right\} \\ &- \frac{\nu \mathcal{P}_\beta}{\chi T_c^{\nu+1} R_h} \left\{ \frac{1}{2\pi \nu} \int_0^\eta s^3 \left(1 - \frac{s}{\eta} \right) (1-s^2)^{-1-1/\nu} ds - b_\nu^{-1} \int_0^\eta s^2 (1-s^2)^{-3/(2\nu)} \int_s^\eta \frac{(1-u^2)^{-1/\nu}}{u^2} dud s \right\}. \end{aligned} \tag{29}$$

As we shall see below, an important quantity governing in particular the ablation rate is the derivative of ϕ at the edge of the hot spot $\eta=1^-$. The first-order approximation gives $\partial_\eta\phi_1(1^-,t)=-\mathcal{D}_n(t)$ with

$$\mathcal{D}_n(t) = \frac{e_\nu}{c_\nu} + \frac{\nu e_\nu \mathcal{P}_\alpha(t)}{\chi T_c^{\nu+1}(t) R_h(t)} \left(\frac{3}{4\pi} - \frac{A_\nu(M(t), T_c(t))}{c_\nu} \right) - \frac{\nu e_\nu \mathcal{P}_\beta(t)}{\chi T_c^{\nu+1}(t) R_h(t)} \left(\frac{3}{4\pi} - \frac{d_\nu}{c_\nu} \right), \quad (30)$$

$$e_\nu = \frac{\sqrt{\pi} \Gamma\left(1 - \frac{1}{\nu}\right)}{4\Gamma\left(\frac{5}{2} - \frac{1}{\nu}\right)}. \quad (31)$$

If nuclear reactions and bremsstrahlung can be neglected, then $\mathcal{D}_n(t) = e_\nu/c_\nu$ is constant. The effect of bremsstrahlung is to decrease \mathcal{D}_n , while the effect of nuclear reactions is usually to increase \mathcal{D}_n . Note that, if $f_\alpha \equiv 1$ and α -particles are locally deposited ($M=0$), then $3/(4\pi) - A_\nu/c_\nu = 0$ and thus $\mathcal{D}_n(t)$ is still equal to e_ν/c_ν . The enhancement due to nuclear reactions is all the more important as $M(t)$ is larger, in which case the energy of the α -particles is deposited at the edge of the hot spot and A_ν takes its minimal value

$$A_\nu(M, T) \simeq \frac{1}{4\pi} \left[\frac{\nu}{\nu-1} - \frac{3\sqrt{\pi} \Gamma\left(1 - \frac{1}{\nu}\right)}{4\Gamma\left(\frac{5}{2} - \frac{1}{\nu}\right)} \right].$$

This means that it is important to take into account a correct model for the energy deposition to capture the value of \mathcal{D}_n .

D. The ablation front

In the previous subsections, we described the hot spot profiles in the asymptotic framework where the temperature in the shell is evanescent. In this subsection, we study more carefully the thin layer that separates the hot spot from the cold shell whose temperature is $T_{\text{sh}}(t)$. We introduce $\delta = T_{\text{sh}}(0)/T_c(0)$ and we study the thin layer in the asymptotic framework $\delta \ll 1$. This asymptotic analysis follows the lines of the one performed in Ref. 4. The temperature profile around the edge of the hot spot has the local form

$$T(t, r) = T_{\text{sh}}(t) \psi^{1/\nu} \left[\frac{r - R_h(t)}{L_0(t)} \right]. \quad (32)$$

The identification of the thickness $L_0(t)$ and the normalized microscopic profile $\psi(\eta)$ can be carried out by substituting Eq. (32) into Eqs. (4) and (5), and by considering that the microscopic profile (32) must match the macroscopic profiles, that is,

$$T^\nu(t, r) \simeq \mathcal{D}_n(t) T_c^\nu(t) \frac{R_h(t) - r}{R_h(t)}$$

for $L_0(t) \ll R_h(t) - r \ll R_h(t)$ and $T(t, r) \simeq T_{\text{sh}}(t)$ for $L_0(t) \ll r - R_h(t) \ll R_h(t)$. Upon substitution, we find that the thickness of the thin layer is of order δ^ν and given by

$$L_0(t) = \frac{\nu}{\mathcal{D}_n(t)} \left[\frac{T_{\text{sh}}(t)}{T_c(t)} \right]^\nu R_h(t), \quad (33)$$

while the normalized profile $\psi(\eta)$ satisfies

$$\frac{\partial \psi}{\partial \eta} = \nu (\psi^{-1/\nu} - 1). \quad (34)$$

The mass flow at the edge of the hot spot is

$$\dot{m}(t) = \frac{\mathcal{D}_n(t) \chi T_c^\nu(t)}{\nu \gamma C_\nu R_h(t)}, \quad (35)$$

which is independent of the precise definition of the position of the edge, i.e., the mass flow is locally constant. An important point is that the mass flow is proportional to $\mathcal{D}_n(t)$, which shows that this parameter is relevant for characterizing the hot spot profile. When nuclear reactions become important and α -particles are deposited in the vicinity of the edge of the hot spot, the parameter $\mathcal{D}_n(t)$ and the ablation rate increase. The same comment holds true for the Froude number $F_r = V_a^2/(g L_0)$, where $V_a = \dot{m}/\rho_{\text{sh}}$ is the ablation velocity and $g = \ddot{R}_h$ is the acceleration:

$$F_r(t) = \mathcal{D}_n^3(t) \frac{(\gamma - 1)^2 \chi^2 T_c^{3\nu}(t)}{\gamma^2 \nu^3 R_h^3 \ddot{R}_h(t) \rho_{\text{sh}}^2(t) T_{\text{sh}}^{\nu-2}(t)}.$$

The velocity flow can be described around the edge of the hot spot by

$$u(t, r) = \dot{R}_h(t) - \frac{c_\nu(\gamma - 1) \chi T_c^\nu(t)}{\nu \gamma \rho_h(t) R_h(t)} T(t, r). \quad (36)$$

To lowest order in δ , the velocity is $\dot{R}_h(t)$. The correction is of order δ . This correction is important since it is the one that is related to ablation. The density-gradient scale length is $L_g = |\rho/\partial_r \rho|$. From the differential equation (34) satisfied by ψ , it is easy to establish that the minimum density-gradient scale length is reached at the point where the temperature is equal to $[(\nu+1)/\nu] T_{\text{sh}}(t)$ and

$$L_{g,\text{min}}(t) = \frac{(\nu+1)^{\nu+1}}{\nu^\nu} L_0(t). \quad (37)$$

Note that this result is consistent with the one obtained by Kull with the well-known isobaric model.¹² The expressions of the mass flow, the Froude number, and the minimum density-gradient scale length are important because they are important parameters in the growth rates of Rayleigh–Taylor instabilities.^{13,14}

E. Validation of the large- ν approximation

In the absence of nuclear reaction and bremsstrahlung, a self-similar flow can be exhibited, which gives a way to compute exactly the solution.⁴ One finds that the profile ϕ satisfies the ordinary differential equation (ODE)

$$c_\nu^{(\text{self})} \frac{1}{\eta^2} \frac{\partial}{\partial \eta} \left(\eta^2 \frac{\partial \phi}{\partial \eta} \right) + \phi^{-1/\nu} = 0, \quad (38)$$

with the boundary conditions $\phi(0)=1$ and $\phi(1)=0$. The constant $c_\nu^{(\text{self})}$ can be determined by a shooting method. For ν

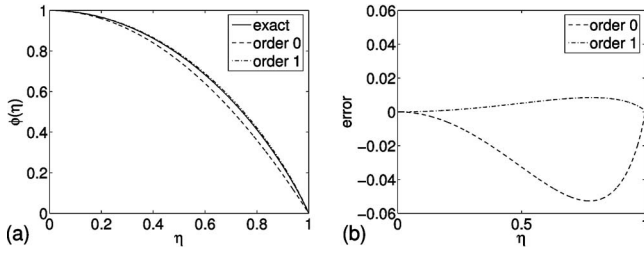


FIG. 3. (a) Spatial profiles of the conductivity in the case $\nu=5/2$. We compare the exact self-similar profile with the zero-order approximation $\phi_0(\eta) = 1 - \eta^2$ and the first-order approximation $\phi_1(\eta)$ given by Eq. (39). (b) Errors between the n th approximations, $n=0, 1$, and the self-similar profile.

$=5/2$, we find $c_{5/2}^{(\text{self})} = 0.197$, which is very close to the value $c_{5/2} = 0.203$ exhibited here above [Eq. (26)].

We can also compare the spatial profiles of the conductivity. The function ϕ at first order is given by Eq. (29), which reads

$$\phi_1(\eta) = 1 - \frac{1 - \frac{1}{\eta} \int_0^\eta (1-s^2)^{1-1/\nu} ds}{1 - \int_0^1 (1-s^2)^{1-1/\nu} ds}. \quad (39)$$

The comparison with the self-similar profile ϕ solution of Eq. (38) shows that the first-order approximation is very accurate (see Fig. 3). In particular, the derivative of the function ϕ at $\eta=1$ plays an important role in the ablation process. It is equal to $\partial_\eta \phi(1^-) = -2.96$ for the self-similar flow, and the first-order approximation gives $\partial_\eta \phi_1(1^-) = -\mathcal{D}_n = -e_\nu / c_\nu = -3.10$. These comparisons seem to prove that the large- ν analysis can be applied to the case $\nu=5/2$.

IV. EFFECTIVE EQUATIONS

By Eqs. (17), (20), and (24), $M(t)$, $\mathcal{P}_\alpha(t)$, and $\mathcal{P}_\beta(t)$ are known functions of $T_c(t)$, $R_h(t)$, and $p_h(t)$. Therefore, Eqs. (8) and (25) are two independent ODEs that give two relations between R_h , p_h , and T_c . In order to get a closed system, a shell model should be adopted. The shell models proposed in Refs. 2–5 give an additional relation between R_h and p_h , in the form of a system of ODEs. Therefore, the final result reads as a closed system of ODEs giving in particular the hot spot pressure $p_h(t)$, the hot spot radius $R_h(t)$, and the central hot spot temperature $T_c(t)$.

Let us give a brief review of the different shell models proposed in the literature. The first model, the so-called thin-shell model, was proposed in Ref. 2. It consists in approximating the shell by a thin and incompressible layer of high-density material.² The shell motion is then deduced from Newton's law, which provides the additional equation $M_{\text{sh}} \ddot{R}_h = 4\pi R_h^2 p_h$, which closes the system (here, M_{sh} is the shell mass). This simple model gives reasonable qualitative predictions, and we will use it to estimate the hot spot velocity during the expansion phase (after stagnation) in Sec. V. It was used for the analysis of the deceleration phase in Ref. 2, but as discussed in Ref. 3, the comparisons with numerical simulations do not exhibit quantitative agreement. The main reason is that shells are thick and compressible in ICF, and a return shock is created at the edge of the hot spot and travels

through the shell, which is not a uniform medium anymore but exhibits two regions with different characteristics. In Ref. 3, a thick shell model is introduced that takes into account the return shock in the cold unperturbed shell, but is limited to special density and velocity profiles in the shell. This model is refined in Refs. 4 and 5 to take into account arbitrary initial profiles for the density and affine profiles for the velocity inside the shell.

The thick shell model proposed in Ref. 5 takes into account the return shock in the cold unperturbed shell. The deceleration phase actually starts when the shock reflected from the center of the capsule interacts with the incoming shell. We thus consider that the shock starts at time 0 from the edge of the hot spot and propagates within the shell. We denote by R_h the hot spot radius and by R_s the shock position. Three regions can be distinguished:

- (1) $r < R_h(t)$ corresponds to the hot spot.
- (2) $R_h(t) < r < R_s(t)$ corresponds to the shocked shell.
- (3) $r > R_s(t)$ corresponds to the cold unperturbed shell, whose pressure is much lower.

Let us first consider the outer region $r > R_s(t)$. The shell is in free-fall conditions with an evanescent pressure and the flow is supersonic. At time 0, the density profile ρ_0 can be arbitrary and we assume that the velocity profile u_0 is affine,

$$\rho_0(r) = \frac{M_{\text{sh}}}{4\pi r^2 \Delta_0} \bar{\rho}_0 \left(\frac{r - R_0}{\Delta_0} \right), \quad (40)$$

$$u_0(r) = -V_{\text{imp}} \frac{\Delta_0 - \eta_0(r - R_0)}{\Delta_0}, \quad (41)$$

where $V_{\text{imp}} (>0)$ is the implosion velocity, M_{sh} is the initial shell mass, R_0 is the initial inner radius of the shell (i.e., the initial position of the shock and the initial radius of the hot spot), and Δ_0 is the initial thickness of the shell. The normalized profile $\bar{\rho}_0$ is such that $\bar{\rho}_0(x) = 0$ for $x \leq 0$, $\bar{\rho}_0(x) > 0$ for $x > 0$, and $\int_0^\infty \bar{\rho}_0(x) dx = 1$. We can neglect heat flow and nuclear reactions inside the free-fall shell. Therefore, it is possible to solve the Euler equations and to get that, for $r > R_s(t)$,

$$\rho_{\text{ff}}(t, r) = \frac{M_{\text{sh}}}{4\pi r^2 \Delta(t)} \bar{\rho}_0 \left(\frac{r + V_{\text{imp}} t - R_0}{\Delta(t)} \right), \quad (42)$$

$$u_{\text{ff}}(t, r) = -V_{\text{imp}} \frac{\Delta_0 - \eta_0(r - R_0)}{\Delta(t)}, \quad (43)$$

$$\Delta(t) = \left(1 + \eta_0 \frac{V_{\text{imp}} t}{\Delta_0} \right) \Delta_0. \quad (44)$$

We denote by M_{ss} the shocked shell mass and $U_h = \dot{R}_h$. With the simple thick shell model described in Ref. 4, we obtain the following closed system of ODEs for the six variables $(R_h, p_h, R_s, M_{\text{ss}}, T_c, U_h)$:

$$\dot{R}_h = U_h, \quad (45)$$

$$\dot{p}_h = \frac{3(\gamma_h - 1)}{4\pi R_h^3} [\mathcal{P}_\alpha(p_h, R_h, T_c) - \mathcal{P}_\beta(p_h, R_h, T_c)] - 3\gamma_h \frac{U_h}{R_h} p_h, \quad (46)$$

$$\dot{R}_s = -\frac{\gamma_s - 1}{2} u_{\text{ff}}(t, R_s) + \frac{\gamma_s + 1}{2} U_h, \quad (47)$$

$$\dot{M}_{\text{ss}} = 4\pi R_s^2 \rho_{\text{ff}}(t, R_s) [\dot{R}_s - u_{\text{ff}}(t, R_s)], \quad (48)$$

$$\begin{aligned} \dot{T}_c = & \frac{\gamma_h - 1}{\gamma_h} \frac{\dot{p}_h}{p_h} T_c - \frac{(\gamma_h - 1)\chi T_c^{\nu+2}}{\gamma_h c_\nu \nu R_h^2 p_h} + \frac{\gamma_h - 1}{\gamma_h c_\nu p_h R_h^3} \\ & \times \{ \mathcal{P}_\alpha(p_h, R_h, T_c) T_c A_\nu [\mathcal{M}(p_h, R_h, T_c), T_c] \\ & - \mathcal{P}_\beta(p_h, R_h, T_c) T_c d_\nu \}, \end{aligned} \quad (49)$$

$$\dot{U}_h = \frac{4\pi R_h^2 p_h}{M_{\text{ss}}} + \frac{\dot{M}_{\text{ss}}}{M_{\text{ss}}} [u_{\text{ff}}(R_s, t) - U_h], \quad (50)$$

where

$$\mathcal{M}(p_h, R_h, T_c) = \frac{2v_{\alpha 0} c_{\alpha e} C_\nu (\gamma - 1) T_c^\nu}{\ln \Lambda_{\alpha e}} \frac{1}{R_h p_h},$$

$$\mathcal{P}_\alpha(p_h, R_h, T_c) = 4\pi \mu_{\alpha d} p_h^2 R_h^3 \int_0^1 f[T_c (1 - \eta^2)^{1/\nu}] \eta^2 d\eta,$$

$$\mathcal{P}_\beta(p_h, R_h, T_c) = \mu_\beta b_\nu p_h^2 R_h^3 T_c^{-3/2}.$$

This model is valid as long as the hot spot mass is smaller than the shell mass. The initial conditions are $R_h(0)=R_0$, $p_h(0)=p_0$, $R_s(0)=R_0$, $M_{\text{ss}}(0)=0$, $T_c(0)=T_0$, and $U_h(0)=0$. The adiabatic exponent is $\gamma_h=5/3$ in the hot spot and $\gamma_s=7/4$ in the shell. It is also possible to use the refined model described in Ref. 5 or any other improved shell model. Once these ODEs have been integrated, the analysis carried out in Refs. 3–5 can be extended, which gives important information such as the hot spot mass, the ablation mass rate, and the density-gradient scale length.

We have considered the approximation (A1) for the fusion cross section, we have numerically integrated the system of ODEs (45)–(50), up to the time when the hot spot mass is 50% of the initial shell mass (which may never occur if ignition does not take place), and we plot the results in Fig. 4. We first apply this model to the baseline Laser Megajoule (LMJ) indirectly driven target:^{15,16} The values of the parameters are $p_0=0.6$ Gbar, $R_0=120$ μm , $V_{\text{imp}}=390$ $\mu\text{m}/\text{ns}$, $M_{\text{sh}}=0.31$ mg, and $\Delta_0=80$ μm . One can see the following from Fig. 4:

- (1) The parameter M takes values larger than 1, which means that the energy of the α -particles is deposited at the edge of the hot spot.
- (2) The presence of bremsstrahlung delays the ignition time [compare the solid lines and the dot-dashed lines in Fig. 4(c)].

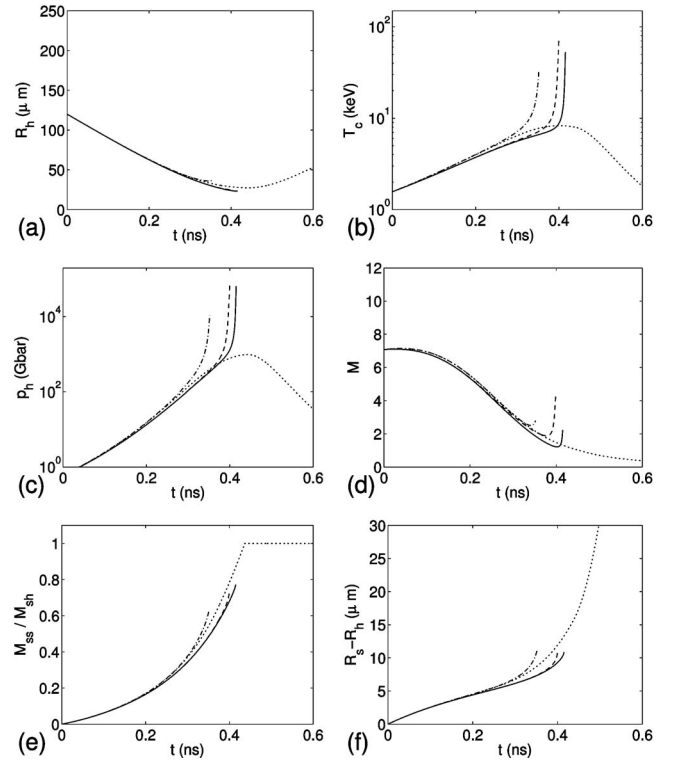


FIG. 4. Hot spot dynamics for the baseline LMJ indirectly driven capsule (nominal implosion velocity). The solid lines stand for the complete model with α -particle transport and bremsstrahlung. The dashed lines stand for local α -particle deposition, the dotted lines for the absence of nuclear reaction, and the dot-dashed lines for the absence of bremsstrahlung.

- (3) The α -particle deposition model has a noticeable effect: At the beginning of ignition (that is, in the early moments when nuclear reactions are important), the central hot spot temperature is reduced compared to the local deposition model [compare the solid lines and the dashed lines in Fig. 4(b)]. This is expected as the α -particles are deposited at the edge of the hot spot, so that the additional heating due to nuclear reaction is first located in this region. It is also noticeable that the pressure increase is slightly reduced compared to the local deposition model at the beginning of ignition. We can explain this by the fact that the central hot spot, where α -particles are generated, is less hot and therefore slightly fewer particles are generated, which involves this slight pressure decay. However, for this capsule, this effect is just transitory, because it is noticeable in Figs. 4(b) and 4(c) that, after this initial central temperature and pressure reduction, the central temperature and pressure increase more strongly with the transport model rather than with the local deposition model at ignition. This can be explained once again by the fact that α -particles are deposited at the edge of the hot spot, which induces more ablation [since $\mathcal{D}_n(t)$ increases], and eventually the nuclear reactions become more important.

In the case described in Fig. 4, bremsstrahlung seems to help ignition. In fact, this is a matter of timing: the implosion of the LMJ capsule has been tuned by full one-dimensional numerical simulations (including bremsstrahlung effects).

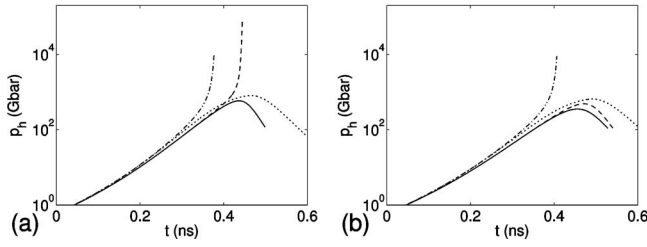


FIG. 5. Hot spot pressure for the same configuration as in Fig. 4, but with reduced implosion velocities [$V_{\text{imp}}=330 \mu\text{m/ns}$ in (a), $V_{\text{imp}}=310 \mu\text{m/ns}$ in (b)].

Changing the modeling of the deceleration phase (by suppressing bremsstrahlung) disturbs the tuning, and the target parameters are not optimized anymore. If we go to marginally ignited shells by dramatically reducing the implosion velocity to $310 \mu\text{m/ns}$ [Fig. 5(b)], then we can see that bremsstrahlung can prevent ignition from occurring: Whatever the deposition model, no ignition occurs, while it occurs in absence of bremsstrahlung (dot-dashed lines). Let us note that for this illustration, the model is applied to the DT shell alone, without taking into account the remaining mass of ablator surrounding the shell in order to prevent from radiation preheating of the solid DT during the acceleration phase (M_{tot} is around $1.25M_{\text{sh}}$ for the nominal LMJ capsule, as described in Ref. 17). This approximation modifies the dependence on implosion velocity of the capsule gain.

The deposition model has a marginal effect for the case described in Fig. 4: The central hot spot temperature and pressure first increase more slowly, and then more strongly with the transport model compared to the local deposition model as explained above. However, the deposition model can have a dramatic effect if the design is marginally close to ignition. If we consider a new configuration with implosion velocity to $330 \mu\text{m/ns}$ [Fig. 5(a)], then ignition occurs with the local deposition model, but not with the transport model. This is due to the fact that the central hot spot temperature increases more slowly with the transport model, because the α -particles are deposited at the edge of the hot spot. As a result, in Fig. 4, the ignition is slightly delayed, but is then stronger because of the enhancement of the ablation process. In Fig. 5(a), the delay is just sufficient to prevent from ignition.

Finally, we consider the directly driven NIF target described in Ref. 2 and we plot the results in Fig. 6. Here $p_0=0.9 \text{ Gbar}$, $R_0=240 \mu\text{m}$, $V_{\text{imp}}=385 \mu\text{m/ns}$, $M_{\text{sh}}=0.31 \text{ mg}$. The qualitative behavior is similar to the previous target.

V. IGNITION CRITERION

In this section, we show how the ideas developed in the previous analysis can be used to derive an ignition criterion that refines the usual Lawson's criterion in terms of the total areal density and the hot spot ion temperature at stagnation.^{1,3,18} Here we are mainly interested in scaling relations, and we will see that some constants should be fixed by numerical simulations (or experiments). We make the assumption that at the beginning of the expansion phase, the temperature (or equivalently the density) profile is approxi-

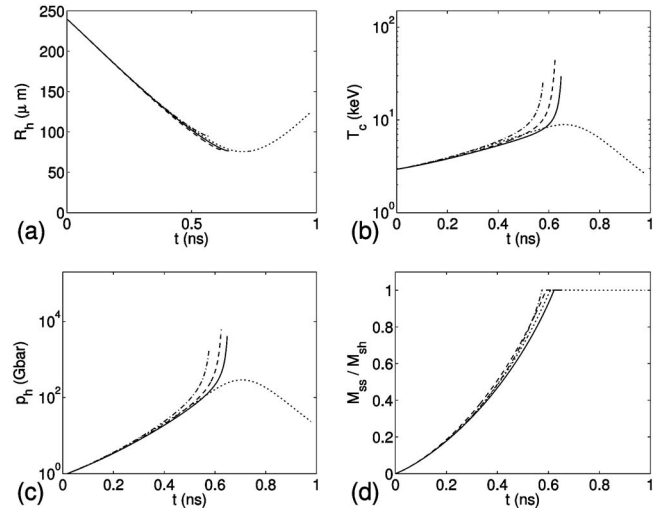


FIG. 6. Hot spot dynamics for the directly driven NIF target.

mately spatially uniform in the hot spot, $T(t, r) \approx T_h(t)$. Alternatively, a self-similar hypothesis for the temperature profile could be assumed. Using the uniform temperature hypothesis, the nuclear reaction rate is also approximately spatially uniform and the total power produced by nuclear reaction and deposited inside the hot spot is

$$\mathcal{P}_\alpha(t) = \mu_\alpha \frac{4\pi R_h^3(t)}{3} p_h^2(t) f_\alpha[T_h(t)]. \quad (51)$$

The total power radiated by electron bremsstrahlung is

$$\mathcal{P}_\beta(t) = \mu_\beta \frac{4\pi R_h^3(t)}{3} p_h^2(t) T_h^{3/2}(t). \quad (52)$$

The energy of the hot spot is

$$\mathcal{E}_h(t) = \frac{4\pi R_h^3(t)}{3(\gamma_h - 1)} p_h(t).$$

Its time evolution is

$$\dot{\mathcal{E}}_h = \frac{4\pi}{\gamma_h - 1} \left[\frac{R_h^3}{3} \dot{p}_h + p_h R_h^2 \dot{R}_h \right],$$

which gives with Eq. (8) $\dot{\mathcal{E}}_h = \mathcal{P}_\alpha - \mathcal{P}_\beta - \mathcal{P}_e$, where $\mathcal{P}_e = 4\pi p_h R_h^2 \dot{R}_h$ is the loss due to expansion ($\dot{R}_h > 0$ during the expansion phase). We therefore obtain

$$\frac{\dot{\mathcal{E}}_h}{\mathcal{E}_h} = (\gamma_h - 1) \left[\mu_\alpha p_h f_\alpha(T_h) - \mu_\beta p_h T_h^{3/2} - \frac{3\dot{R}_h}{R_h} \right]. \quad (53)$$

The ignition criterion is that the energy balance of the hot spot at the beginning of the expansion phase is positive $\dot{\mathcal{E}}_h > 0$, which reads

$$\mu_\alpha p_h f_\alpha(T_h) - \mu_\beta p_h T_h^{3/2} > \frac{3\dot{R}_h}{R_h}.$$

It appears necessary to have an estimate of the ratio \dot{R}_h/R_h . For this, we adopt the thin shell model during the expansion phase: $M_{\text{sh}} \ddot{R}_h = 4\pi R_h^2 p_h$, and assume that M_{sh} is constant. The

thin shell model is reasonable here since the target is designed so that the entire shell is shocked at the stagnation time. This second-order equation is not sufficient to estimate \dot{R}_h . If, additionally, we assume that we are close to the ignition threshold, that is to say, the ignition criterion is just satisfied, then we also have $\dot{\mathcal{E}}_h/\mathcal{E}_h \simeq 0$ and therefore $\partial_t(p_h R_h^3) \simeq 0$. This gives

$$\begin{aligned} M_{\text{sh}} \frac{d}{dt}(\dot{R}_h^2) &= 2M_{\text{sh}} \ddot{R}_h \dot{R}_h = 8\pi p_h R_h^2 \dot{R}_h \\ &= 8\pi (p_h R_h^3) \frac{d}{dt}(\ln R_h), \end{aligned}$$

and therefore

$$\frac{\dot{R}_h}{R_h} = \left[\frac{8\pi R_h p_h}{M_{\text{sh}}} \ln\left(\frac{R_h}{R_0}\right) \right]^{1/2},$$

where R_0 is the hot spot radius at stagnation. The $\sqrt{\ln}$ term is slowly varying when $R_h \in (1.1R_0, 2R_0)$ and can be substituted by a constant, say $1/2$, which gives

$$\frac{\dot{R}_h}{R_h} \simeq \left(\frac{4\pi p_h R_h}{M_{\text{sh}}} \right)^{1/2}. \quad (54)$$

Obviously, the constant should be fitted by numerical simulations. Therefore, the ignition criterion reads

$$\frac{p_h^{1/2} M_{\text{sh}}^{1/2}}{R_h^{1/2}} f(T_h) > \frac{6\sqrt{\pi}}{\mu_\alpha},$$

where the function $f(T_h)$ is defined by

$$f(T_h) = f_\alpha(T_h) - \frac{\mu_\beta T_h^{-3/2}}{\mu_\alpha}. \quad (55)$$

A rough estimate of the shell mass M_{sh} in terms of the shell density ρ_s and the shell thickness Δ_s is $M_{\text{sh}} \simeq 4\pi\rho_s\Delta_s R_h^2$. The EOS also gives $p_h = C_v(\gamma_h - 1)\rho_h T_h$, so we obtain the ignition criterion in terms of the three quantities $\rho_h R_h T_h$, $\rho_s \Delta_s$, and T_h ,

$$(\rho_h R_h T_h)^{1/2} (\rho_s \Delta_s)^{1/2} f(T_h) > \frac{3}{\mu_\alpha (\gamma_h - 1)^{1/2} C_v^{1/2}}. \quad (56)$$

The function $f(T_h)$ is plotted in Fig. 7. It is negative for $T_h < 4.3$ keV, which means that ignition is not permitted in this region.

The areal density $\rho_s \Delta_s$ and the hot spot temperature T_h are measurable quantities in ICF experiments, but $\rho_h R_h$ is usually not directly accessible. It is possible to use the fact that the shell that the hot spot has to push in order to expand is the one that has given energy to the hot spot during the deceleration phase, and that the hot spot energy at stagnation comes from the conversion of this kinetic energy, $(1/2)M_{\text{sh}}V_{\text{imp}}^2 = 4\pi/[3(\gamma_h - 1)]R_h^3 p_h$, where V_{imp} is the implosion velocity. Using once again the EOS and the relation $M_{\text{sh}} = 4\pi\rho_s\Delta_s R_h^2$, we obtain $\rho_h T_h R_h = (3V_{\text{imp}}^2)/(2C_v)\rho_s\Delta_s$, and we finally get the criterion

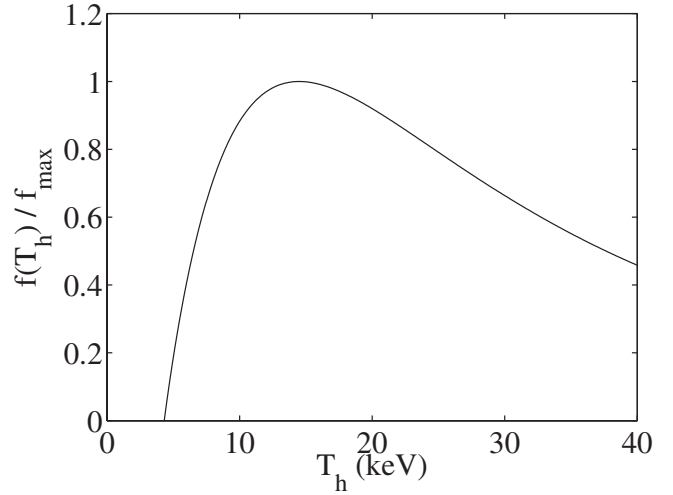


FIG. 7. Function $f(T_h)$ normalized by its maximal value, using the parameters given in Appendix A.

$$(\rho_s \Delta_s) V_{\text{imp}} f(T_h) > \frac{\sqrt{6}}{\mu_\alpha (\gamma_h - 1)^{1/2}}. \quad (57)$$

A similar formula was recently proposed by Betti and Zhou^{19,20} [in the case $f_\alpha(T) = T$], and fitted by numerical simulations for the direct drive configuration. A detailed study of our criterion based on a more accurate fusion model will be the subject of a forthcoming paper.

VI. CONCLUSION

In this paper, we have obtained a closed system of ordinary differential equations that governs the evolution of the main hydrodynamic quantities of the hot spot during the deceleration phase of an ICF capsule. These equations take into account the energy released by nuclear reactions, a nonlocal model for the α -particle energy deposition process, bremsstrahlung effects, and a nonlinear heat conductivity model with a Spitzer exponent ν that is assumed to be large. By comparing the predictions of these equations in some special cases in which self-similar solutions are known, we show that the exponent $\nu = 5/2$ is large enough to ensure the validity of the results. By considering a baseline LMJ capsule, we show that α -particle transport and radiation loss by bremsstrahlung play a quantitative role. Bremsstrahlung delays the ignition time, which may not occur at all if the delay is large enough so that stagnation is reached first. A correct model for α -particle transport is also important, because it turns out that in the early moments when nuclear reactions occur, the α -particles are generated inside the hot spot but deposited at the edge of the hot spot. In particular, we show that, compared to the simple model in which the deposition is uniform in the hot spot, the deposition of the α -particles at the edge of the hot spot can slightly delay the ignition time (or even prevent from ignition if the delay is too long), but it can also enhance the ignition process by increasing the ablation rate.

Contrary to previous papers, the introduction of free parameters for the shell dynamics and for the nuclear energy deposition is not needed in our model. Indeed, the thin shell model is widely used, but since only the shocked part of the

shell participates in the compression of the hot spot, it is usually necessary to introduce a free parameter that can be interpreted as the fraction of shocked shell mass in order to calibrate the shell dynamics. Besides, α -particle transport is usually not taken into account, so that a free parameter that can be interpreted as the absorbed α -particle fraction is normally introduced in order to calibrate the nuclear energy deposition. In our work, these free parameters are not present anymore.

The detailed analysis given in this paper concerns the deceleration phase, the stagnation phase and is valid up to the beginning of the expansion phase. Beyond this time, the complete phenomenology of thermonuclear burn should be taken into account, in particular the fractional burnup, the scattering of the α -particles, the depletion of the fuel, its expansive disassembly, the spherical thermonuclear burn wave propagating from the central hot spot in the shell, and the separation between the electronic, ionic, and radiative temperatures.^{7,21}

APPENDIX A: NUMERICAL VALUES

The following values are taken from Ref. 1:

- (1) The fusion cross section can be approximated by the formula

$$\langle\sigma v\rangle = 9.1 \times 10^{-16} \times \exp\left[-0.572 \left|\ln\left(\frac{T}{64.2}\right)\right|^{2.13}\right] \text{ cm}^3 \text{ s}^{-1}, \quad (\text{A1})$$

with T expressed in keV, which is accurate to 10% in the range 3–100 keV and to 20% in the range 0.3–3 keV.

- (2) The parameters of the α -particles with the energy $E_\alpha = 3500$ keV are $v_{\alpha 0} = 1.29 \times 10^9$ cm s⁻¹ and $A_\alpha = 8 \times 10^{40}$ erg g⁻².
- (3) The parameters of the α -particle transport model are $\ln \Lambda_{\alpha e} = 5$ and $c_{\alpha e} = 4.2 \times 10^{-11}$ s keV^{-3/2} g cm³.
- (4) The parameters of the ideal EOS for the gaseous hot spot are $\gamma = 5/3$ and $C_v = 1.15 \times 10^{15}$ erg g⁻¹ keV⁻¹.
- (5) The parameters of the Spitzer conductivity model are $\nu = 5/2$ and $\chi = 1.9 \times 10^{19}$ erg s⁻¹ cm⁻¹ keV^{-7/2}.
- (6) The parameter of the bremsstrahlung radiation loss is $a_b = 3.05 \times 10^{23}$ erg cm³ g⁻² s⁻¹ keV^{-1/2} and $\lambda_p = 14.4$ cm⁻⁵ g² keV^{-7/2}.

APPENDIX B: ENERGY DEPOSITED BY AN α -PARTICLE

Let us consider an α -particle emitted at time t_0 , radial position $r = r_0$, with the velocity $v_{\alpha 0}$ and the angle ψ with respect to the outward radial direction. This particle travels through the inhomogeneous plasma whose temperature profile is Eq. (14). Its velocity decreases as

$$\frac{dv}{dt} = -\frac{v}{1 - \frac{R_h^2}{r^2}} \frac{1}{T_\alpha}, \quad \frac{1}{T_\alpha} = \frac{\ln \Lambda_{\alpha e}}{2c_{\alpha e} C_v (\gamma - 1) T_c^\nu}.$$

The travel time of an α -particle is much smaller than the characteristic time of variations of the hydrodynamic quan-

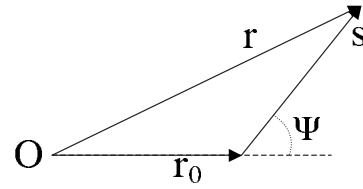


FIG. 8. The starting point of the α -particle has radial position r_0 , the emission angle is ψ , the traveled distance at time t is $s(t)$, and the radial position at time t is $r(t)$.

ties R_h , T_c , and p_h , so we can assume that these quantities are frozen at t_0 . The radial position $r(t)$ is related to the traveled distance $s(t)$ by $r^2 = r_0^2 + 2sr_0 \cos \psi + s^2$ as shown in Fig. 8.

The velocity is $v(t) = ds/dt$. Therefore, we get the differential equation

$$\frac{d^2 s}{dt^2} = -\frac{ds}{dt} \frac{1}{T_\alpha} \frac{R_h^2}{R_h^2 - r_0^2 - 2sr_0 \cos \psi - s^2}.$$

The α -particle is emitted with the initial velocity $v_{\alpha 0}$ and it stops when its velocity vanishes, that is, when the particle has traveled the distance s_f given by

$$\int_0^{s_f} \frac{R_h^2}{R_h^2 - r_0^2 - 2sr_0 \cos \psi - s^2} ds = v_{\alpha 0} T_\alpha,$$

which corresponds to the radial position $r_f^2 = s_f^2 + 2s_f r_0 \cos \psi + r_0^2$. After some algebra, we get that the radial position of the stopping point is

$$r_f(t_0, r_0, \psi) = R_h(t_0) \eta_f \left[t_0, \frac{r_0}{R_h(t_0)}, \psi \right],$$

$$\eta_f^2(t_0, \eta_0, \psi) = \eta_0^2 \sin^2 \psi + N_f^2 (1 - \eta_0^2 \sin^2 \psi),$$

$$N_f = \frac{\eta_0 \cos \psi + T_f \sqrt{1 - \eta_0^2 \sin^2 \psi}}{T_f \eta_0 \cos \psi + \sqrt{1 - \eta_0^2 \sin^2 \psi}},$$

$$T_f = \tanh[\sqrt{1 - \eta_0^2 \sin^2 \psi} M(t_0)],$$

where $M(t_0)$ is defined by (20).

The kinetic energy of the α -particle is deposited along the path that goes from the emission point to the stopping point. In order to get the energy deposited along the path, the velocity of the particle along the path needs to be computed. The results are as follows:

- (1) If $\cos \psi \geq 0$, then $r_f > r_0$, the radial position increases from r_0 to r_f , and the velocity $v = ds/dt$ along the path is

$$v(r) = v_{\alpha 0} \tilde{v}_+ \left[\frac{r}{R_h(t_0)} \right],$$

$$\tilde{v}_+(\eta) = 1 - \frac{1}{M(t_0)} \frac{1}{\sqrt{1 - \eta_0^2 \sin^2 \psi}} \operatorname{arctanh}[Q_+(\eta)],$$

$$Q_+(\eta) = \frac{\sqrt{1 - \eta_0^2 \sin^2 \psi} (\eta_0 \cos \psi - \sqrt{\eta^2 - \eta_0^2 \sin^2 \psi})}{\eta_0 \cos \psi \sqrt{\eta^2 - \eta_0^2 \sin^2 \psi} - (1 - \eta_0^2 \sin^2 \psi)}.$$

(2) If $\cos \psi < 0$ and

$$\sqrt{1 - \eta_0^2 \sin^2 \psi} \tanh[\sqrt{1 - \eta_0^2 \sin^2 \psi} M(t_0)] + \eta_0 \cos \psi \leq 0, \tag{B1}$$

then the radial position decreases from r_0 to r_f and the velocity along this path is

$$v(r) = v_{\alpha 0} \tilde{v}_- \left[\frac{r}{R_h(t_0)} \right],$$

$$\tilde{v}_-(\eta) = 1 + \frac{1}{M(t_0)} \frac{1}{\sqrt{1 - \eta_0^2 \sin^2 \psi}} \operatorname{arctanh}[Q_-(\eta)],$$

$$Q_-(\eta) = \frac{\sqrt{1 - \eta_0^2 \sin^2 \psi} (\eta_0 \cos \psi + \sqrt{\eta^2 - \eta_0^2 \sin^2 \psi})}{\eta_0 \cos \psi \sqrt{\eta^2 - \eta_0^2 \sin^2 \psi} + (1 - \eta_0^2 \sin^2 \psi)}.$$

(3) If $\cos \psi < 0$ and Eq. (B1) does not hold, then the radial position decreases from r_0 to $r_{\min} := R_h(t_0) \eta_{\min}$,

$$\eta_{\min} = \eta_0 \sin \psi,$$

and the velocity along this path is $v(r) = v_{\alpha 0} \tilde{v}_- [r/R_h(t_0)]$. Next the radial position increases from r_{\min} to r_f and the velocity is then given by $v_{\alpha 0} \tilde{v}_+ [r/R_h(t_0)]$.

We can now give the expression of the energy deposited by the particle. The energy deposited in the annulus $[r, r + dr]$ is $e(r; r_0, t_0, \psi) dr$ with the energy density

$$e(r; r_0, t_0, \psi) = \frac{m_i v_{\alpha 0}^2}{2 R_h(t_0)} \tilde{e} \left[\frac{r}{R_h(t_0)}; \frac{r_0}{R_h(t_0)}, t_0, \psi \right].$$

If $\cos \psi \geq 0$, the energy is deposited between r_0 and r_f with the density

$$\tilde{e}(\eta; \eta_0, t_0, \psi) = -2\tilde{v}_+(\eta) \frac{d\tilde{v}_+(\eta)}{d\eta} \mathbf{1}_{[\eta_0, \eta_f]}(\eta).$$

(2) If $\cos \psi < 0$ and Eq. (B1) holds, then the energy is deposited between r_f and r_0 with the density

$$\tilde{e}(\eta; \eta_0, t_0, \psi) = 2\tilde{v}_-(\eta) \frac{d\tilde{v}_-(\eta)}{d\eta} \mathbf{1}_{[\eta_f, \eta_0]}(\eta).$$

(3) If $\cos \psi < 0$ and Eq. (B1) does not hold, then the energy is deposited along the (decaying) path from r_0 to r_{\min} , and then along the (increasing) path from r_{\min} to r_f ,

$$\begin{aligned} \tilde{e}(\eta; \eta_0, t_0, \psi) = & -2\tilde{v}_-(\eta) \frac{d\tilde{v}_-(\eta)}{d\eta} \mathbf{1}_{[\eta_{\min}, \eta_0]}(\eta) \\ & + 2\tilde{v}_+(\eta) \frac{d\tilde{v}_+(\eta)}{d\eta} \mathbf{1}_{[\eta_{\min}, \eta_f]}(\eta). \end{aligned}$$

Note that the initial energy of the α -particle is $m_i v_{\alpha 0}^2 / 2$ and that it is totally deposited inside the hot spot, so that for any $\eta_0 \in [0, 1]$, ψ , and t_0 , we have $\int_0^1 \tilde{e}(\eta; \eta_0, t_0, \psi) d\eta = 1$.

¹S. Atzeni and J. Meyer-ter-Vehn, *The Physics of Inertial Fusion* (Clarendon Press, Oxford, 2004).
²R. Betti, M. Umansky, V. Lobatchev, V. N. Goncharov, and R. L. McCrory, *Phys. Plasmas* **8**, 5257 (2001).
³R. Betti, K. Anderson, V. N. Goncharov, R. L. McCrory, D. D. Meyerhofer, S. Skupsky, and R. P. J. Town, *Phys. Plasmas* **9**, 2277 (2002).
⁴J. Garnier and C. Cherfils-Cl erouin, *Phys. Plasmas* **12**, 012704 (2005).
⁵J. Sanz, J. Garnier, C. Cherfils, B. Canaud, L. Masse, and M. Temporal, *Phys. Plasmas* **12**, 112702 (2005).
⁶J. Sanz and R. Betti, *Phys. Plasmas* **12**, 042704 (2005).
⁷P. Gauthier, F. Chaland, and L. Masse, *Phys. Rev. E* **70**, 055401 (2004).
⁸C. Almarcha, P. Clavin, L. Duchemin, and J. Sanz, *J. Fluid Mech.* **579**, 481 (2007).
⁹V. N. Goncharov, Ph.D. thesis, University of Rochester, 1998.
¹⁰J. H. Hammer and M. D. Rosen, *Phys. Plasmas* **10**, 1829 (2003).
¹¹Y. Saillard, *Nucl. Fusion* **46**, 1017 (2006).
¹²H. J. Kull, *Phys. Fluids B* **1**, 170 (1989).
¹³J. Sanz, *Phys. Rev. Lett.* **73**, 2700 (1994).
¹⁴V. N. Goncharov, R. L. Betti, R. L. McCrory, P. Sorotokin, and C. P. Verdon, *Phys. Plasmas* **3**, 1402 (1996).
¹⁵Y. Saillard, *C. R. Acad. Sci., Ser IV: Phys., Astrophys.* **1**, 705 (2000).
¹⁶P. A. Holstein, M. Andre, M. Casanova, F. Chaland, C. Charpin, C. Cherfils, L. Divol, H. Dumont, D. Galmiche, J. Giorla, L. Hallo, S. Laffite, L. Lours, M. C. Monteil, D. Mourenas, F. Poggi, Y. Saillard, G. Schurtz, M. Valadon, D. Vanderhaegen, and F. Wagon, *C. R. Acad. Sci., Ser IV: Phys., Astrophys.* **1**, 693 (2000).
¹⁷Y. Saillard, *Laser Part. Beams* **22**, 451 (2004).
¹⁸M. C. Hermann, M. Tabak, and J. D. Lindl, *Nucl. Fusion* **41**, 99 (2001).
¹⁹C. D. Zhou and R. Betti, *Phys. Plasmas* **14**, 072703 (2007).
²⁰R. Betti and C. D. Zhou, *Bull. Am. Phys. Soc.* **52**, 63 (2007).
²¹G. S. Fraley, E. J. Linnebur, R. J. Mason, and R. Morse, *Phys. Fluids* **17**, 474 (1974).